

# Characterization of atmospheric turbulence for LEO to ground laser beam propagation at low elevation angles

Nicolas Védrenne, Marie-Thérèse Velluet, Vincent Michau

Theoretical and Applied Optics Department  
ONERA, The French Aerospace Lab  
92322 Châtillon Cedex, France  
[Nicolas.vedrenne@onera.fr](mailto:Nicolas.vedrenne@onera.fr)

Géraldine Artaud, Frédéric Lacoste  
DCT/RF/ITP  
CNES  
18, av. Edouard Belin,  
31401 Toulouse Cedex 9, France

Etienne Samain, Clément Courde  
OCA-Géoazur  
2130, Route de l'Observatoire,  
06460 Saint-Vallier-de-Thiery, France

**Abstract**— Data transfer from Low Earth Orbit satellites to ground implies the availability of communication link at various elevations. Increasing the overall downlink capacity implies communication even at low elevation angle. Optical laser link throughput capacities are highly dependent on propagation conditions. Unfortunately these conditions are more severe at low elevations due to a longer path in the turbulent atmosphere. Dedicated mitigation strategies have to be developed to address propagation channel impairments. But the choice of the technique and its efficiency depends on our knowledge of the perturbations. In the small perturbations regime analytical formalism has been developed to describe the statistical properties of the perturbations. However, at low elevation angles, analytical formalism can no longer be exploited. In the saturation regime heuristic approaches have been proposed. However, wave optics models are the most powerful tool to estimate the impact of atmospheric turbulence whatever the perturbations. Nevertheless, different questions have to be answered to develop such a code: spatial sampling of phase screens, longitudinal sampling of the turbulence profile along the line of sight... Whereas propagation conditions are well documented for elevation angles above 30°, few measurements have been made and published for elevations below. The present paper reports experimental measurements of turbulence characteristics. They were recorded in the visible spectrum using stars as sources. Elevation angles down to 10° were addressed. These measurements were performed with a fast Shack-Hartmann wavefront sensor, installed at the Coudé focus of the MeO laser telescope at Cote d'Azur observatory during summer 2013. Atmospheric turbulence characteristics (spatial and temporal spectra of scintillation and phase) are estimated from the measurements and compared to wave optics results.

**Keywords**—wavefront sensing, scintillation, laser beam propagation, wave optics.

## I. INTRODUCTION

Laser communications are currently envisaged for high data rate payload telemetry of the future Earth Observation missions. Indeed, they offer significant improvements compared to classical radio-frequency communications: increased data rates with reduced power consumption, mass and size [1]. However, free space optical communications links are significantly impaired by the propagation through

atmosphere and in particular the atmospheric turbulence. The minimum elevation angle for which such optical links are studied is basically 20° due to link budget constraints [2]. Considering lower minimum elevation angles, down to 10°, could offer increased visibility times (factor 2 if clouds are omitted) and then increased links capacity. Nevertheless, considering such very low elevation angles makes the atmospheric turbulence more problematic compared with elevation angles higher than 30°. In order to assess the performance of Earth-Space high data rate transmission through optical links, for example at 1.55 μm, ONERA developed for CNES an automatic parameterized wave optics model: TURANDOT [3]. This physical model, optimized in terms of computation time in the small perturbations regime has to be assessed for elevation angles below 30° since it often corresponds to strong perturbations regime. For doing so, the light coming from bright stellar sources has been recorded for both high and low elevation angles in a short lapse of time using the MeO telescope of Côte d'Azur observatory (Southern France) [4]. Acquisitions were performed by nighttime and daytime. The statistical characteristics of the perturbations caused by turbulence have then been analysed for both elevations and compared to wave optics results. For the estimation of wave optics parameters ( $C_n^2$  profile and wind profile), measurements at high elevation angles were used according to the following process. Stellar scintillation characteristics are well documented for high elevations [5][6][7]. For elevations above 40° the small perturbations approximation is satisfied. Analytical tools that relate integrated turbulence parameters (Fried parameter and scintillation index) to  $C_n^2$  profile and wind profile exist and can be used to adjust parametric models of  $C_n^2$  and wind profiles. These parameters can then be used as inputs of the wave optics model TURANDOT. Wave optics results obtained with these parameters are then compared to measurement results for both high and low elevations. The experimental setup is presented in section II, section III focuses on turbulence parameters estimation. In section IV wave optics results are compared to the measurements.

## II. EXPERIMENTAL SETUP

### A. The MeO Telescope

The MeO station for “Metrology and Optics” is a versatile telescope located in the hinterland of Grasse at an altitude of 1270 meters. The primary activity of the station is artificial satellite and lunar laser ranging. The station participates also to several research programs such as optical time transfer, adaptive optics, high resolution imagery, debris detection, optical telecom and astronomical observation. The station benefits from the best compromise between accessibility and sky quality. The station is based on a 1.5 meter Ritchey-Chretien telescope installed on an Alt-Az mount (see Figure 1). The total weight of the mobile elements of the instrument is 20 tons.

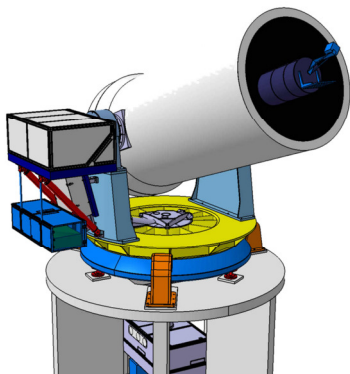


**Figure 1: Overview of the MeO station. Telescope diameter: 1.5 m.**

A 60 m<sup>2</sup> circular coudé focus laboratory located under the telescope is equipped with several optical benches to lead different R&D projects. One bench, in the middle of the room, is devoted to the flux distribution. This bench has a fold mirror on a rotation stage that permits to send the light from the telescope Coudé to one of the other optical benches. The turbulence characterization setup used in this experiment is installed in this room.

The Coudé permits to manipulate the optical beacon coming either from the laser or the telescope. It is made with some large 200 mm flat fold mirror made in Zérodur dielectric coatings. The spectral bandwidth is between 350 to 1100 nm with a reflection factor higher than 98 % for both s and p polarizations.

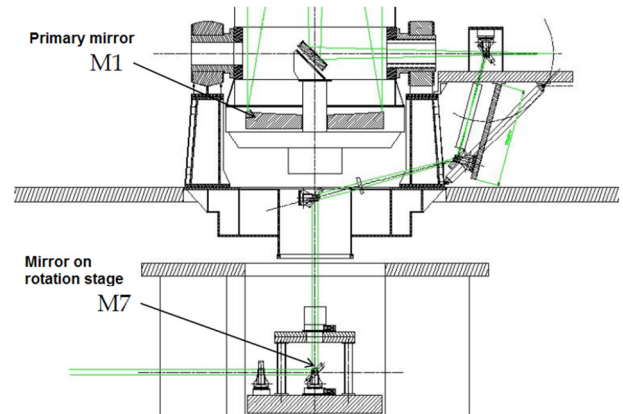


**Figure 2: Description of the coudé path.**

The telescope is able to track any targets in the sky at a maximum speed of 5°/s. The mount works with direct drive motors and direct encoders for both azimuthal and elevation axes. The main characteristics are:

- Motor torque: 10000 N.m
- Pointing repeatability error: 0.1 arcsec
- Pointing accuracy: better than 2 arcsec

The pointing accuracy is obtained through a calibration process using absolute position of stars. This calibration is based on a 6 order harmonic decomposition model built through the observation of 48 stars chosen on the entire celestial sphere.

### B. Turbulence characteristics monitoring

Turbulence monitoring is performed with a wavefront sensor located on a dedicated optical bench after the Coudé focus. The wavefront sensor (WFS) is a Shack Hartmann WFS with 8x8 square subapertures. The size of a subaperture projected into the entrance pupil of the system is 19 cm. The focal plane of each subaperture is sampled with 30x30 pixels. The focal length of the microlenses has been chosen so that Shannon sampling factor is 0.5 at 600 nm (one diffraction spot per pixel). The WFS camera is a First Light Imaging™ OCAM<sup>2</sup> camera with an engineering grade E2V chip of 240x240 pixels. Quantization is performed on 14 bits. Slopes and intensities per subaperture are recorded at a 1500 Hz frequency. A screen shot of a raw image of the focal plane of the CCD is presented in Figure 3. The slope computation algorithm is a thresholded COG. The threshold value is adjusted to limit background noise influence on the slope measurements. Intensities are computed by the addition of the values of pixels higher than the threshold.

For each considered star source, series of 40 000 set of slopes and intensities were acquired. In parallel a ground level measurement of the  $C_n^2$  was performed using thermal probes located at 1 m from ground.

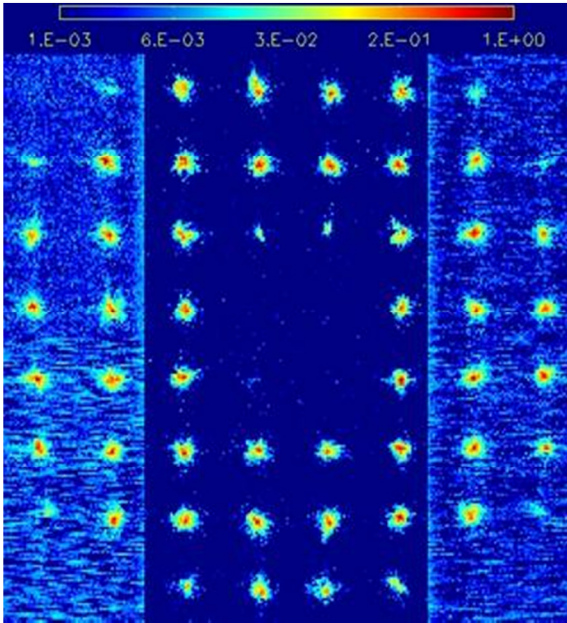


Figure 3: Screen shot of the wavefront sensor focal plane.

C. Stellar sources

Stellar sources have been selected on the basis of their elevation and the available expected flux. By daytime, background signal generated by Rayleigh diffusion in the atmosphere is attenuated using a 80 nm band pass optical filter centered on 600 nm. A photometric budget has been made to estimate the expected flux and SNR. The flux from the star is evaluated from its magnitude and its spectrum given by its classification and a perfect black body model. Atmospheric transmission and background diffusion have been evaluated with a radiative transfer tool called MATISSE [8]. The detected signal is processed, considering a whole transmission of 10% taking into account optical path attenuation and quantum efficiency of the detector. The signal detected for each selected star at the average wavelength of the spectrum  $\lambda_{mean}$ , considering an integration time of 1/1500 s is reported in Figure 4 together with the expected signal to noise ratio (SNR). The signals are expressed in photons at  $\lambda_{mean}$ . SNR is computed assuming that the detection is photon noise limited according to Eq. 1 where  $S_{star}$  is the signal detected from a star and  $S_{background}$  the signal detected from the background (diffusion)

$$SNR = \frac{S_{star} - S_{background}}{\sqrt{S_{star} + S_{background}}}$$

Eq. 1

Star	Elevation (°)	°K	$\lambda_{mean}$ $\mu$ m	kphotons / subaperture @ $\lambda_{mean}$	SNR ( $D/r_0=3$ )
Sirius	28	9600	0.6	20	140
Vega	85	10000	0.6	5.3	65
Arcturus	20 - 40	4460	0.7	4.7	60
Antares	10	3500	0.75	2.9	45
Deneb	73	8400	0.61	1.7	31
Altair	65	8000	0.61	2.5	41

Figure 4: Photometric budget results for the selected stars.

III. MEASUREMENTS

A. Turbulence parameters estimations

From each set of 40.000 slopes, Zernike decomposition on 55 modes is performed and the variances of each radial order are computed. Then, an evaluation of the Fried parameter at 600 nm is performed using a fit of the radial variances by Noll formula [8]. An example of result obtained from slopes acquired on Deneb at 23:19 UT on 13<sup>th</sup> July 2013 is presented in Figure 5. Aliasing effects induce an over excitation of the highest radial orders. Residual vibrations may explain the discrepancy at radial order 1. Consequently, these radial orders are not used for the fit.

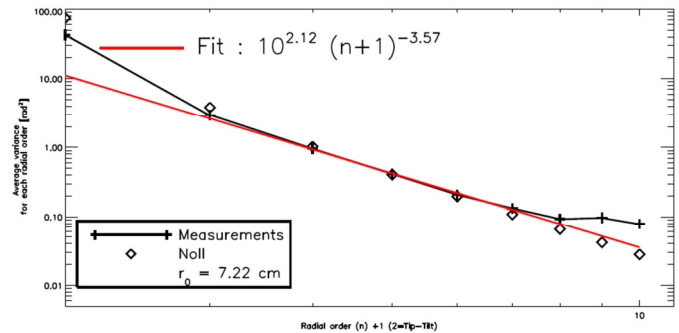


Figure 5: Fit of the Zernike variances by Noll formula on Deneb (13<sup>th</sup> July 2013, 23:19 UT).

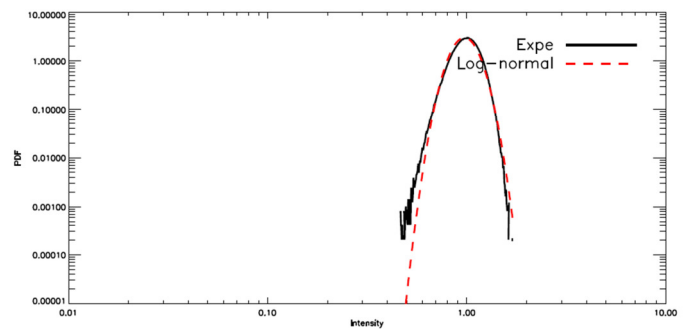


Figure 6: Probability density function of the variations of the flux collected per subaperture on Deneb (13<sup>th</sup> July 2013, 23:19 UT).

The probability density function (PDF) estimated from the flux fluctuations recorded for one subaperture is plotted in Figure 6. The PDF is the average PDF on every non occulted

subaperture. Normalized flux fluctuations ( $i$ ) are computed according to Eq. 2 where  $S$  corresponds to the intensity signal recorded on one subaperture by summation of the intensity of every pixel and  $\langle S \rangle$  is the statistical average of the signal for the subaperture over the whole set :

$$i = \frac{S - \langle S \rangle}{\langle S \rangle}$$

Eq. 2

### B. Measurements results

Measurements of  $r_0$  and normalized flux fluctuations variance  $\sigma_i^2$  for the night of 13<sup>th</sup> July 2013, between 22:32 and 23:39 UT are plotted in Figure 7. Five stars with five different elevations were successively considered: Vega (83°), Arcturus (28°), Altair (53°), Deneb (73°), and Arcturus (22°). As expected, the smaller the elevation is, the higher the flux fluctuations are, due to a longer propagation path through the turbulent atmosphere.

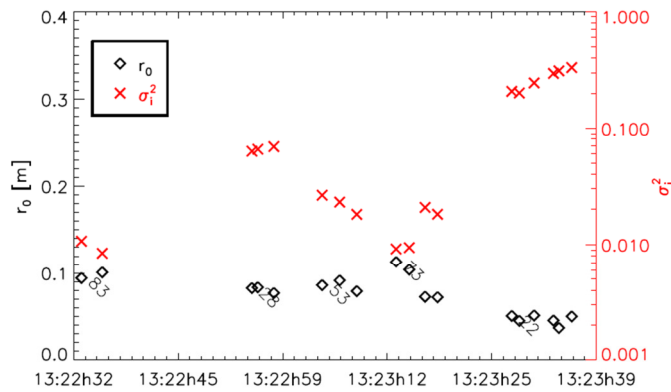


**Figure 7:  $r_0$  and flux fluctuations variances for the 5 stars studied between 22:32 and 23:39 the 13th July 2013.**

## IV. EXPLOITATION

### A. Wave optics parametrization

In this section the measurements are confronted to wave optics results for low elevations. Wave optics modeling requires the knowledge of the  $C_n^2$  and wind profiles.

A  $C_n^2$  vertical profile model is implemented in the wave optics tool [3]. This model corresponds to a 5/7 Hufnagel-Valley profile [10] for high altitude layers. For low altitude layers,  $C_n^2$  decreases with a similitude power law in  $h^p$  where  $p = 2/3$  for a stable atmosphere (typically by nighttime) and  $p = 4/3$  (typically by daytime)[1][12]. The parameters of the  $C_n^2$  model are the  $C_n^2$  at ground level and the stability condition. The vertical wind profile model implemented in the wave optics tool is a Bufton wind profile. Its parameters are the wind velocities at ground level and for the high altitude layer and the altitude of the high altitude layer.

The parameters of the profiles are estimated from the data recorded at high elevations by using analytical models valid in the small perturbations regime. In the following, the vertical profiles are assumed to be unchanged whatever the elevation.

This assumption seems reasonable considering the limited sensitivity of the simulation results to these profiles.

To ensure that the small perturbation approximation is satisfied two conditions are monitored. The first one is that the probability density function (PDF) of flux fluctuations collected by each subaperture follows a log-normal law. The second one is the value of the Rytov log-amplitude variance is smaller than 0.3. PDF for two elevations are presented on the left of Figure 8 (black lines): 73° on the top of the figure, 22° on the bottom. The log-normal PDF obtained with flux fluctuations variance estimated from the measured PDF is plotted in green. It appears that for the high elevation case the log-normal model fits well the data, whereas this is not true for the low elevation case. The computed Rytov log-amplitude variance considering the aperture averaging effect is 0.06 for 73° and 0.5 for 22°. It appears here that the previously cited conditions are well satisfied for the high elevation case and are not for the low elevation case.

As the small perturbations approximation is satisfied for the 73° case, analytical models of  $r_0$  and  $\sigma_i^2$  can be exploited.

Considering a stability compatible with a nighttime observation and a  $C_n^2$  at ground level equal to  $10^{-14} \text{ m}^{-2/3}$  (value compatible with the thermal probes), turbulence parameters are  $r_0 = 9 \text{ cm}$  and  $\sigma_i^2 = 0.020$ , to be compared to the measurements that are  $r_0 = 7 \text{ cm}$  and  $\sigma_i^2 = 0.024$ .

The wind profile model parameters are adjusted so that the analytical model of flux fluctuations temporal power spectral density (TPSD) [13] fits the measured TPSD for the high elevation case. The result of the best fit is the green curve of the upper right corner of Figure 8. The parameters of the Bufton wind profile are indicated in the legend.

### B. Simulation results and comparison to experiment

Using the estimated parameters, wave optics simulations are performed for the two elevations. A set of 4000 time samples of flux fluctuations are simulated for a total simulated duration of 6 seconds. PDF and TPSDs from numerical simulation results are plotted in Figure 8 (red crosses).

Considering the TPSDs, simulation results are close to the analytical evaluations even for the low elevation case. As perturbations are increased, specific spatial frequencies appear in the speckle pattern at the receiver aperture plane. Using an aperture greater than the size of these speckles extends the validity of the small perturbations approximation due to averaging effect as long as Rytov limit is only slightly exceeded. This explains why analytical developments based on the small perturbations approximation are still valid here.

Considering the PDFs, simulation results and measurements are very similar. They both reproduce the log-normal PDF for the high elevation case. For the low elevation case the log-normal model is no longer satisfied due to stronger perturbations, whereas the wave optics tool delivers results consistent with experiments. This demonstrates that the log-normal model cannot reproduce the growing influence of multiple scattering that occurs when perturbations are increased. To take into account the modification of the PDF, more sophisticated models exist [14]. However they require

specific adjustments that restrict their domain of validity and make their use application dependent. This illustrates the limit of currently available analytical tools when it comes to turbulence simulation for low elevations line of sights.

To analyze experiment results, rather crude hypothesis on the  $C_n^2$  profile and on the wind profile were made. However, the simulation results seem rather close to the measurements in terms of statistical characteristics. This tends to demonstrate that the sensitivity of these statistical characteristics to the turbulence vertical distribution is limited, particularly for low elevation angles.

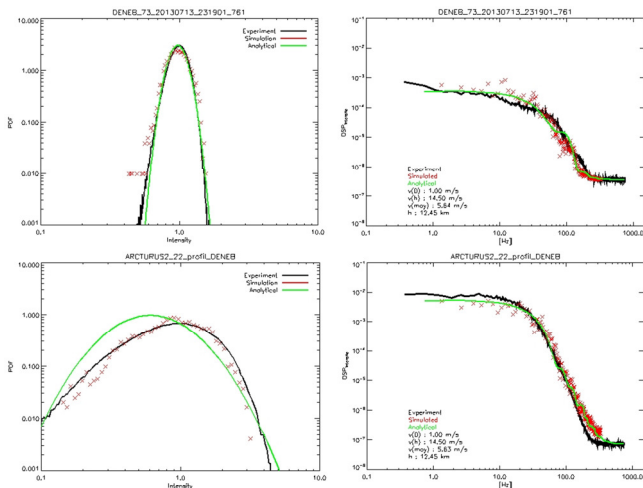


**Figure 8: Top: statistical characteristics of flux fluctuations for high elevation (73°, Deneb, 23:19). Bottom: low elevation (22°, Arcturus, 23:36). Left: Probability densities function, right: temporal power spectral density.**

## V. CONCLUSION

Measurements of stellar scintillation and wavefront slopes in the visible were conducted in July 2013 at the Côte d'Azur Observatory. The aim was to gather measurements to be compared to wave optics results. As they correspond to small perturbations, high elevation measurements were used to estimate the parameters of the wave optics tool. Once the parameters were estimated, they were used to simulate turbulence induced perturbations. The statistical characteristics of the numerical model results show good agreement with the measurements, especially for low elevation angles, whereas analytical tools based on small perturbations theory are no longer reliable. It appears with this work that statistical

characteristics of flux fluctuations for low elevation show a limited sensitivity to  $C_n^2$  and wind profile.

## ACKNOWLEDGMENT

This work has been performed thanks to financial support of CNES in the framework of its R&T research program.

## REFERENCES

- [1] A.Guérin, G.Lesthievant, J.-L.Issler, "Evaluation of new technological concepts for high data rate payload telemetry", 5th ESA TTC workshop, Noordwijk, The Netherlands, September 2010.
- [2] A.Guérin, F.Lacoste, A.Laurens, G.Azema, C.Periard, D.Grimal, "Optical links capacity for LEO satellites over European ground networks", ITC 2010, San Diego, USA, October 2010.
- [3] N. Vedrenne, J.-M. Conan, M.-T. Velluet, M. Sechaud, M. Toyoshima, H. Takenaka, A. Guérin, F. Lacoste, "Turbulence effects on bi-directional ground-to-satellite laser communication systems", ICSOS 2012, Ajaccio, France, October 2012
- [4] E. Samain, A. Abchiche, D. Albanese, et al. "MeO: The new French lunar laser station. In Proceedings of the 16th International Workshop on Laser Ranging", October, 2008.
- [5] Ochs, G. R., Wang, T. I., Lawrence, R. S., & Clifford, S. F., "Refractive-turbulence profiles measured by one-dimensional spatial filtering of scintillations", Applied optics, 15(10), 2504-2510, 1976.
- [6] Frehlich, R. G., "Estimation of the parameters of the atmospheric turbulence spectrum using measurements of the spatial intensity covariance", Applied optics, 27(11), 2194-2198, 1988.
- [7] Tokovinin, A., "Turbulence profiles from the scintillation of stars, planets, and Moon", in Workshop on Astronomical Site Evaluation (Eds. I. Cruz-González, J. Echevarría & D. Hiriart) (Vol. 31, pp. 61-70), 1988.
- [8] C.Schweitzer, K.Stein, N.Wendelstein, L.Labarre, K.Caillaut, S.Fauqueux, C.Malherbe, A.Roblin, B.Rosier, P.Simoneau, "Validation of the background simulation model MATISSE : comparing results with MODIS satellite images", Proc. of SPIE Vol. 817805.
- [9] R. Noll, "Zernike polynomials and atmospheric turbulence," J. Opt. Soc. Am. 66, 207-211, 1976.
- [10] R.-E. Hufnagel, "Variations of atmospheric turbulence," in Proc. Of Topical Meeting on Optical Propagation through the Turbulence, 1974.
- [11] A. Monin and A. Obukhov, Basic turbulent mixing laws in the atmospheric surface layer. Trudy Geofiz. Inst. AN SSSR, 1954.
- [12] J. C. Wyngaard, Y. Izumi, and S. A. Collins, Jr., "Behavior of the Refractive-Index -Structure Parameter near the Ground," J. Opt. Soc. Am., 61, 1646-1650, 1971.
- [13] Robert, C., Conan, J. M., Michau, V., Renard, J. B., Robert, C., & Dalaudier, "Retrieving parameters of the anisotropic refractive index fluctuations spectrum in the stratosphere from balloon-borne observations of stellar scintillation", JOSA A, 25(2), 379-393, 2008.
- [14] Andrews, Larry C., and Ronald L. Phillips. "Laser beam propagation through random media", 1998.